Abstracta

Ano XXIII - N. 01

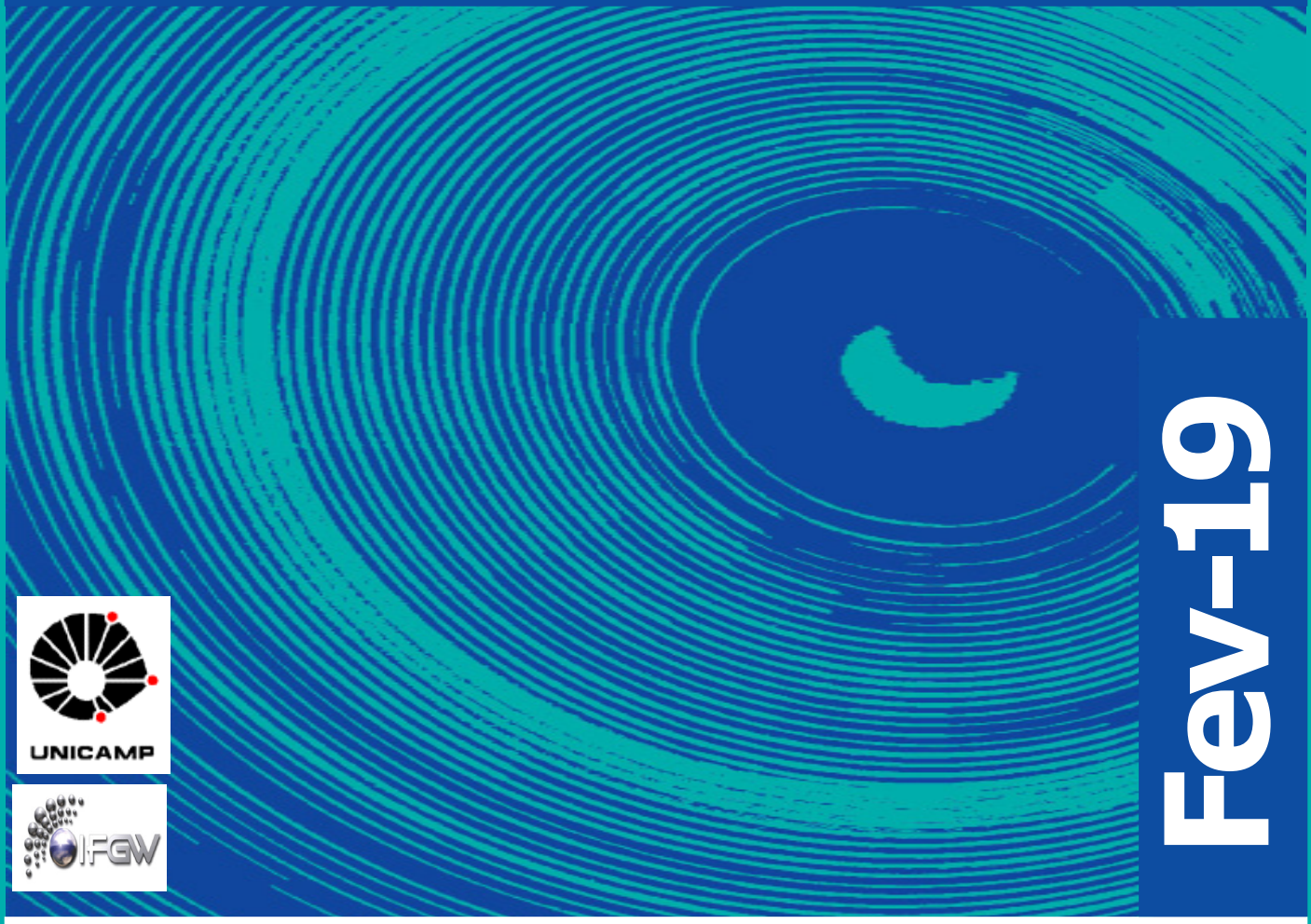

Fev-19

UNICAMP

IFGW

Artigos publicados 2018 - P460-2018 à P491-2018

Eventos publicados 2018 - P492-2018 à P494-2018

Artigos publicados 2019 - P001-2019 à P021-2019

Artigos aceitos para publicação - A001-2019

Defesas de Dissertações do IFGW - D001-2019

Artigos publicados 2018

[P460-2018] "A new fabrication process of pedestal waveguides based on metal dielectric composites of Yb3+ /Er3+ codoped PbO-GeO2 thin films with gold nanoparticles"

Bomfim, F. A.; Rangel, R. C.; da Silva, D. M.; Carvalho, D. O.; **Melo, E. G.***; Alayo, M. I.; Kassab, L. R. P.

This work reports the signal enhancement of Yb3+/Er3+ codoped PbO-GeO2 pedestal waveguides due to gold nanoparticles deposited over the core layer. The pedestal structure was obtained by conventional photolithography and plasma etching with a new procedure that does not use metallic hard-masks that normally introduce roughness, leading to light scattering. This new procedure brings advantages that benefit light guiding, reducing the propagation losses. Yb (3+)/Er3+ codoped PbO-GeO2 thin film was obtained by RF Magnetron Sputtering deposition and was used as core layer (410 nm height). In order to cover the core with gold nanoparticles the sputtering technique was used, followed by annealing at 400 degrees C during 1 h. The minimum propagation losses obtained were of 1.0 dB/cm at 1068 nm. Scanning Electron Microscopy (SEM) was employed for the waveguides structure inspection and transmission electronic microscopy (TEM) was used to verify the presence of gold nanoparticles on the waveguides. It was observed an enhancement of 180% for the relative gain that reached 7.8 dB/cm at 1530 nm, for an optical waveguide with 6 pm core width, under 980 nm excitation (pump power of 60 mW), attributed to the local field enhancement in the vicinity of the gold nanoparticles. The new fabrication process presented in this work opens possibilities for optical amplifiers with low propagation losses based on different metal dielectric composites, as well as other waveguide-based devices.

OPTICAL MATERIALS 86, 433-440, 2018. DOI: 10.1016/j.optmat.2018.10.044

[P461-2018] "A short travel for neutrinos in Large Extra Dimensions"

Stenico, G. V.*; Forero, D. V.*; Peres, O. L. G.*

Neutrino oscillations successfully explain the flavor transitions observed in neutrinos produced in natural sources like the center of the sun and the earth atmosphere, and also from man-made sources like reactors and accelerators. These oscillations are driven by two mass-squared differences, solar and atmospheric, at the sub-eV scale. However, longstanding anomalies at short-baselines might imply the existence of new oscillation frequencies at the eV-scale and the possibility of this sterile state(s) to mix with the three active neutrinos. One of the many future neutrino programs that are expected to provide a final word on this issue is the Short-Baseline Neutrino Program (SBN) at FERMILAB. In this letter, we consider a specific model of Large Extra Dimensions (LED) which provides interesting signatures of oscillation of extra sterile states. We started re-creating sensitivity analyses for sterile neutrinos in the 3+1 scenario, previously done by the SBN collaboration, by simulating neutrino events in the three SBN detectors from both muon neutrino disappearance and electron neutrino appearance. Then, we implemented neutrino oscillations as predicted in the LED model and also we have performed sensitivity analysis to the LED parameters. Finally, we studied the SBN power of discriminating between the two models, the 3+1 and the LED. We have found that SBN is sensitive to the oscillations predicted in the LED model and have the potential to constrain the LED parameter space better than any other oscillation experiment for m(1)(D) < 0.1 eV. In case SBN observes a departure from the three active neutrino framework, it also has the power of discriminating between sterile oscillations predicted in the 3+1 framework and the LED ones.

JOURNAL OF HIGH ENERGY PHYSICS 11, 155, 2018. DOI: 10.1007/JHEP11(2018)155

[P462-2018] "An MHD Effect on a Newtonian Fluid Flow Due to a Superlinear Stretching Sheet"

Kumar, P. N. V.; Mahabaleshwar, U. S.; **Sakanaka, P. H.***; Lorenzini, G.

The preliminary aim of this article is to investigate the effect of magnetohydrodynamic (MHD) flows of a viscous fluid due to a superlinear stretching sheet. These boundary layer flows arise in the industrial processes such as polymer extrusion processes, metal spinning, glass blowing and heat exchangers. The representing frameworks of highly nonlinear partial differential equations are mapped to nonlinear ordinary differential equations with a constant coefficient via similarity transformation and are solved analytically. The results are analyzed by means of various plots to provide the comparison and found to be in better agreement with the classical results of Crane and Pavlov. The viscous fluid due to a superlinear stretching sheet in the presence ofMHDhas enormous amount of nonlinearity in conducting the solution area with different arrangements.

JOURNAL OF ENGINEERING THERMOPHYSICS 27[4] 501-506, 2018. DOI: 10.1134/S1810232818040112

[P463-2018] "Angular analysis of the decay B+ -> K+mu(+) mu(-) in proton-proton collisions at root s=8 TeV"

Sirunyan, A. M.; Tumasyan, A.; **Chinellato, J. A.*; Tonelli Manganote, E. J.***; et al.
CMS Collaboration

The angular distribution of the flavor-changing neutral current decay B+ -> K+mu(+)mu(-) is studied in proton-proton collisions at a center-of-mass energy of 8 TeV. The analysis is based on data collected with the CMS detector at the LHC, corresponding to an integrated luminosity of 20.5 fb(-1). The forward-backward asymmetry A(FB) of the dimuon system and the contribution F-H from the pseudoscalar, scalar, and tensor amplitudes to the decay width are measured as a function of the dimuon mass squared. The measurements are consistent with the standard model expectations.

PHYSICAL REVIEW D, 98[11], 112011, 2018. DOI: 10.1103/PhysRevD.98.112011

[P464-2018] "Carbon Nanotubes for Quantum Dot Photovoltaics with Enhanced Light Management and Charge Transport"

Tazawa, Y.; Habisreutinger, S. N.; Zhang, N.; Gregory, D. A. F.; **Nagamine, G.***; Kesava, S. V.; Mazzotta, G.; Assender, H. E.; Riede, M.; Padilha, L. A.*; Nicholas, R. J.; Watt, A. A. R.

Colloidal quantum dot (CQD)-based photo-voltaics are an emerging low-cost solar cell technology with power conversion efficiencies exceeding 10%, i.e., high enough to be interesting for commercialization. Well-controlled and understood charge carrier transport through the device stack is required to make the next step in efficiency improvements. In this paper, polymer-wrapped single-walled carbon nanotube (SWNT) films embedded in an insulating poly(methyl methacrylate) (PMMA) matrix and capped by a thermally evaporated Au electrode are investigated as a composite hole transport layer and optical spacer. Employing transient absorption spectroscopy we show that the SWNTs enhance the charge transfer rate from CQD to CQD, ZnO, or SWNT.

In order to pinpoint the underlying mechanism for the improvement, we investigate the energetics of the junction by measuring the relative alignment of the band edges, using Kelvin probe and cyclic voltammetry. Measuring the external quantum efficiency and absorption we find that the improvement is not mainly from electronic improvements but from enhanced absorption of the CQD absorber. We demonstrate experimentally and theoretically, by employing a transfer-matrix model, that the transparent PMMA matrix acts as an optical spacer, which leads to an enhanced absorption in the absorber layer. With these electronic and optical enhancements, the efficiency of the PbS CQD solar cells improved from 4.0% to 6.0%.

ACS PHOTONICS 5[12], 4854-4863, 2018. DOI: 10.1021/acsphotonics.8b00982

[P465-2018] "Characterization of surface-states in a hollow core photonic crystal fiber"

Lamilla, E.*; Faria, M. S.*; Aldaya, I.*; Jarschel, P. F.*; Pita, J. L.*; Dainese, P.*

Surface or edge states represent an important class of modes in various photonic crystal systems such as in dielectric topological insulators and in photonic crystal fibers. In the later, strong attenuation peaks in the transmission spectrum are attributed to coupling between surface and core-guided modes. Here, we explore a modified implementation of the spatial and spectral interference method to experimentally characterize surface modes in photonic crystal fibers. Using an external reference and a non-uniform Fourier transform windowing, the obtained spectrogram allows clear observation of anti-crossing behavior at wavelengths in which surface and core modes are strongly coupled. We also detect surface modes with different spatial symmetries, and give insight into mode families couple to the fundamental or high-order core modes, as well as the existence of uncoupled surface modes.

OPTICS EXPRESS 26[25], 32554-32564, 2018. DOI: 10.1364/OE.26.032554

[P466-2018] "Event shape variables measured using multijet final states in proton-proton collisions at root s=13 TeV"

Sirunyan, A. M.; Tumasyan, A.; **Chinellato, J. A.*; Tonelli Manganote, E. J.***; et al.
CMS Collaboration

The study of global event shape variables can provide sensitive tests of predictions for multijet production in proton-proton collisions. This paper presents a study of several event shape variables calculated using jet four momenta in proton--proton collisions at a centre-of-mass energy of 13 TeV and uses data recorded with the CMS detector at the LHC corresponding to an integrated luminosity of 2.2 fb(-1). After correcting for detector effects, the resulting distributions are compared with several theoretical predictions. The agreement generally improves as the energy, represented by the average transverse momentum of the two leading jets, increases.

JOURNAL OF HIGH ENERGY PHYSICS 12, 117, 2018. DOI: 10.1007/JHEP12(2018)117

[P467-2018] "Evidence for the Associated Production of a Single Top Quark and a Photon in Proton-Proton Collisions at root s=13 TeV"

Sirunyan, A. M.; Tumasyan, A.; **Chinellato, J. A.*; Tonelli Manganote, E. J.***; et al.
CMS Collaboration

The first evidence of events consistent with the production of a single top quark in association with a photon is reported. The analysis is based on proton-proton collisions at root s = 13 TeV and recorded by the CMS experiment in 2016, corresponding to an integrated luminosity of 35.9 fb(-1). Events are selected by requiring the presence of a muon (mu), a photon (gamma), an imbalance in transverse momentum from an undetected neutrino (nu), and at least two jets (j) of which exactly one is identified as associated with the hadronization of a b quark. A multivariate discriminant based on topological and kinematic event properties is employed to separate signal from background processes. An excess above the backgroundonly hypothesis is observed, with a significance of 4.4 standard deviations. A fiducial cross section is measured for isolated photons with transverse momentum greater than 25 GeV in the central region of the detector. The measured product of the cross section and branching fraction is sigma(pp -> t gamma j) B (t -> mu nu b) = 115 +/- 17 (stat) +/- 30(syst) fb, which is consistent with the standard model prediction.

PHYSICAL REVIEW LETTERS 121[22], 221802, 2018. DOI: 10.1103/PhysRevLett.121.221802

[P468-2018] "Influence of pH and ionic strength on the antibacterial effect of hyaluronic acid/chitosan films assembled layer-by-layer"

Nascimento, V.; Franca, C.; **Hernandez-Montelongo, J.***; Machado, D.; Lancellotti, M.; **Cotta, M.*; Landers, R.***; Beppu, M.

Hyaluronic acid (HA)/chitosan (CHI) films were assembled by LbL using different conditions of pH and ionic strength (IS) in order to obtain stable surfaces to avoid the adhesion and proliferation of Pseudomonas aeruginosa and Staphylococcus aureus. The results showed that pH and IS were key synthesis variables for obtaining different features, such as wettability, thickness and the availability of functional groups. The antibacterial effect was more effective against S. aureus with a reduction of approximately 3, 4, and 1.5 log reduction after 4, 8 and 24 h of culture time, respectively. In the case of P. aeruginosa, the films presented a lower bacterial reduction: 1 log reduction in times evaluated. In conclusion, the results of the antibacterial effect against S. aureus after 24 h, suggest that the HA/CHI films assembled by LbL can protect several substrates, such as biomedical devices, against bacterial proliferation.

EUROPEAN POLYMER JOURNAL 109, 198-205, 2018. DOI: 10.1016/j.eurpolymj.2018.09.038

[P469-2018] "Magnetic nanocomposites based on shape memory polyurethanes"

Soto, G. D.; Meiorin, C.; Actis, D. G.; Mendoza Zelis, P.; **Londono, O. M.*; Muraca, D.***; Mosiewicki, M. A.; Marcovich, N. E.

Shape memory composites based on a commercial segmented polyurethane and magnetite (Fe3O4) nanoparticles (MNPs) were prepared by a simple suspension casting method. The average sizes of individual magnetic particles/clusters were determined by TEM microscopy and corroborated from SAXS patterns. The magnetization properties of selected samples were evaluated using zero field cooling/field cooling (ZFC/FC) measurements and magnetization loops obtained at different temperatures. The results showed that magnetization at high field (20 k Oe) and coercitivity measured at 5 K increase with magnetite content and that all the composite films exhibit superparamagnetic behavior at 300 K. The specific absorption rate (SAR) of the nanocomposites was calculated by experimentally determining both the specific heat capacity and the heating rate of the films exposed to an alternant magnetic field.

All nanocomposites were able to increase their temperature when exposed to an alternant magnetic field, although the final temperature reached resulted dependent of the MNPs concentration. What is more, a fast and almost complete recovery of the original shape of the nanocomposites containing more than 3 nominal wt.% MNP was obtained by this remote activation applied to the previously deformed samples.

EUROPEAN POLYMER JOURNAL 109, 8-15, 2018. DOI: 10.1016/j.eurpolymj.2018.08.046

[P470-2018] "Magnetic Remote Activation of Shape Recovery in Nanocomposites Based on Tung Oil and Styrene"

Meiorin, C.*; Actis, D. G.; Montoro, F. E.; Londono, O. M.; Aranguren, M. I.; **Muraca, D.***; Zelis, P. M.; **Knobel, M.***; Mosiewicki, M. A.

The activation of unconstrained shape recovery in bio-based polymeric nanocomposites is successfully achieved using magnetic nanoparticle heating. The materials investigated in this work present several distinct physical and chemical characteristics worth pointing out: they can be deformed and the original shape can be recovered by remotely heating the samples above their switching temperature, which is determined by their glass transition temperatures. Also, their chemical composition is largely based on biomass (the polymeric matrix contains more than 50 wt.% of raw tung oil). Magnetic heating performance is strongly affected by both the physical properties and the concentration of the nanoparticles loaded into the matrix. The concentration of nanoparticles is associated with the formation of agglomerates or clusters, which determines the dipolar interactions among the nanoparticles. The particles used in this work are able to absorb enough energy from an alternating magnetic field to heat the matrix and initiate the shape recovery. Although the sample with the highest content of magnetic solute (10 wt.%) presents the highest degree of agglomeration, it is also the sample with the best remote activation of shape recovery, according to the temperature reached under magnetothermal measurements and the time of actuation.

PHYSICA STATUS SOLIDI A-APPLICATIONS AND MATERIALS SCIENCE 215[24], 1800311, 2018. DOI: 10.1002/pssa.201800311

[P471-2018] "Measurement of differential cross sections for Z boson production in association with jets in proton- proton collisions at v s=13TeV"

Sirunyan, A. M.; Tumasyan, A.; **Chinellato, J. A.*; Tonelli Manganote, E. J.***; et al.
CMS Collaboration

The production of a Z boson, decaying to two charged leptons, in association with jets in proton- proton collisions at a centre- of- mass energy of 13 TeV is measured. Data recorded with the CMS detector at the LHC are used that correspond to an integrated luminosity of 2.19 fb - 1. The cross section is measured as a function of the jet multiplicity and its dependence on the transverse momentum of the Z boson, the jet kinematic variables (transverse momentum and rapidity), the scalar sum of the jet momenta, which quantifies the hadronic activity, and the balance in transverse momentum between the reconstructed jet recoil and the Z boson. The measurements are compared with predictions from four different calculations. The first two merge matrix elements with different parton multiplicities in the final state and parton showering, one of which includes oneloop corrections. The third is a fixed- order calculation with next- to- next- to- leading order accuracy for the process with a Z boson and one parton in the final state.The fourth combines the fully differential next- to- next- to- leading order calculation of the process with no parton in the final state with next- to- next- to- leading logarithm resummation and parton showering.

EUROPEAN PHYSICAL JOURNAL C 78[11], 965, 2018. DOI: 10.1140/epjc/s10052-018-6373-0

[P472-2018] "Measurement of jet substructure observables in t(t)over-bar events from proton-proton collisions at root s=13 TeV"

Sirunyan, A. M.; Tumasyan, A.; **Chinellato, J. A.*; Tonelli Manganote, E. J.***; et al.
CMS Collaboration

A measurement of jet substructure observables is presented using t (t) over bar events in the lepton + jets channel from proton-proton collisions at root s = 13 TeV recorded by the CMS experiment at the LHC, corresponding to an integrated luminosity of 35.9 fb(-1). Multiple jet substructure observables are measured for jets identified as bottom, light-quark, and gluon jets, as well as for inclusive jets (no flavor information). The results are unfolded to the particle level and compared to next-to-leading-order predictions from POWHEG interfaced with the parton shower generators PYTHIA 8 and HERWIG 7, as well as from SHERPA 2 and DIRE 2. Avalue of the strong coupling at the Z boson mass, alpha(S)(m(Z)) = 0.115(-0.013)(+0.015), is extracted from the substructure data at leading-order plus leading-log accuracy.

PHYSICAL REVIEW D 98[9], 092014, 2018. DOI: 10.1103/PhysRevD.98.092014

[P473-2018] "Measurements of Higgs boson properties in the diphoton decay channel in proton-proton collisions at root s=13 TeV"

Sirunyan, A. M.; Tumasyan, A.; **Chinellato, J. A.*; Tonelli Manganote, E. J.***; et al.
CMS Collaboration

Measurements of Higgs boson properties in the H decay channel are reported. The analysis is based on data collected by the CMS experiment in proton-proton collisions at =13 TeV during the 2016 LHC running period, corresponding to an integrated luminosity of 35.9 fb(-1). Allowing the Higgs mass to float, the measurement yields a signal strength relative to the standard model prediction of 1.18-0.14+0.17=1.18-0.11+0.12(stat)--0.07+0.09(syst)-0.06+0.07(theo), which is largely insensitive to the exact Higgs mass around 125 GeV. Signal strengths associated with the different Higgs boson production mechanisms, couplings to bosons and fermions, and effective couplings to photons and gluons are also measured.

JOURNAL OF HIGH ENERGY PHYSICS 11, 185, 2018. DOI: 10.1007/JHEP11(2018)185

[P474-2018] "Nanoindentation unidirectional sliding and lateral force microscopy: Evaluation of experimental techniques to measure friction at the nanoscale"

Echeverrigaray, F. G.; Sales de Mello, S. R.; Boeira, C. D.; Leidens, L. M.; Maia da Costa, M. E. H.; Freire, F. L., Jr.; **Alvarez, F.***; Michels, A. F.; Figueroa, C. A.

Lateral force microscopy (LFM) is an established technique to assess friction forces at the nanoscale. Nanoindentation followed by unidirectional sliding (NUS) is also used to evaluate friction forces at the micro/nanoscale. However, comparative studies between NUS and LFM evaluating the experimental results at different scales are still missing. In this work, a-C:D/H and a-C:H thin films with different [D]/[C] and [H]/[C] contents were used to analyze the friction forces by NUS and LFM.

The results show that the friction behavior assessed by these two techniques in different scales is the same. The correlation between friction forces measured by NUS and LFM depends mainly on a contact area factor that makes invariant the friction force from nanoscale to microscale. Such behavior suggests a similar damping mechanism, probably phonon-coupling phenomena, for the friction force origin.

AIP ADVANCES 8[12], 125013, 2018. DOI: 10.1063/1.5047801

[P475-2018] "Observation of Medium-Induced Modifications of Jet Fragmentation in Pb-Pb Collisions at root s(NN)=5.02 TeV Using Isolated Photon-Tagged Jets"

Sirunyan, A. M.; Tumasyan, A.; **Chinellato, J. A.*; Tonelli Manganote, E. J.***; et al.
CMS Collaboration

Measurements of fragmentation functions for jets associated with an isolated photon are presented for the first time in pp and Pb-Pb collisions. The analysis uses data collected with the CMS detector at the CERN LHC at a nucleon-nucleon center-of-mass energy of 5.02 TeV. Fragmentation functions are obtained for jets with P-T(jet) 30 GeV/c in events containing an isolated photon with p(T)(gamma) 60 GeV/c, using charged tracks with transverse momentum p(T)(trk) > 1 GeV/c in a cone around the jet axis. The association with an isolated photon constrains the initial p(T) and azimuthal angle of the parton whose shower produced the jet. For central Pb-Pb collisions, modifications of the jet fragmentation functions are observed when compared to those measured in pp collisions, while no significant differences are found in the 50% most peripheral collisions. Jets in central Pb-Pb events show an excess (depletion) of low (high) p(T) particles, with a transition around 3 GeV/c. This measurement shows for the first time the in-medium shower modifications of partons (quark dominated) with well-defined initial kinematics. It constitutes a new well-controlled reference for testing theoretical models of the parton passage through the quark-gluon plasma.

PHYSICAL REVIEW LETTERS 121[24], 242301, 2018. DOI: 10.1103/PhysRevLett.121.242301

[P476-2018] "On higher derivative corrections to the R plus R-2 inflationary model"

Castellanos, A. R. R.*; Sobreira, F.*; Shapiro, I. L.; Starobinskyel, A. A.

The R + R-2 model is successful in describing inflation, as it provides an excellent fit to the full set of available observational data. On the other hand, the same model is the simplest extension of general relativity which does not produce higher derivative ghosts and related instabilities. Long ago, it was proposed to treat all terms which cause higher derivative instabilities as small perturbations that could avoid the presence of ghosts in the spectrum. We put this proposal into practice and consider an explicit example of treating more complicated higher derivative terms as small perturbations over the R + R-2 model by introducing the R square R term into the action. Within the described scheme, it is possible to obtain an upper bound on the coefficient of this non-scale-free sixth-derivative term by mapping the theory into a one-scalar field potential. It is shown that the result differs from treating this term on equal footing with other terms that requires mapping to a two-scalar field model, and in general leads to different observational consequences.

JOURNAL OF COSMOLOGY AND ASTROPARTICLE PHYSICS 12, 007, 2018. DOI: 10.1088/1475-7516/2018/12/007

[P477-2018] "Polymer optical fiber specklegram strain sensor with extended dynamic range"

Fujiwara, E.; **da Silva, L. E.*; Marques, T. H. R.*; Cordeiro, C. M. B.***

A polymer optical fiber strain sensor with extended dynamic range is reported. The proposed algorithm resets the reference fiber status depending on the magnitude of the specklegram deviation so the correlation coefficient never saturates, yielding a continuous response over the full range for both positive and negative strains. The technique was evaluated on the measurement of axial strains using a ZEONEX core, poly(methyl methacrylate) cladding multimode fiber, presenting reproducible results with 3 x 10(-3) mu epsilon(-1) sensitivity (similar to 15 mu epsilon resolution) within a 22,600 mu epsilon interval. In contrast to the available approaches, the presented method can retrieve the strain direction and does not require intensive image processing, thus providing a simple and reliable technique for mechanical measurements using multimode optical fibers.

OPTICAL ENGINEERING 57[11], 116107, 2018. DOI: 10.1117/1.OE.57.11.116107

[P478-2018] "Protein Corona Formation on Magnetic Nanoparticles Conjugated with Luminescent Europium Complexes"

Khan, L. U.; Petry, R.; Paula, A. J.; **Knobel, M.***; Martinez, D. S.T.

The evaluation of the nanoparticles interactions with blood plasma enables a first and important insight on the organization of the adsorbed protein layer. In this context, we studied the formation of protein corona on magneto-luminescent Fe3O4@calix-Eu(TTA) nanoparticles in human plasma. The difference in the surface chemistry of F3O4 functionalized with calixarene (+30 mV zeta-potential) and europium (III) thenoyltrifluoroacetonate (Eu3+-TTA) complex (+7.4 mV zeta-potential) affected the colloidal stability and hard corona composition of the nanoparticles, which were monitored by SDS-PAGE gel electrophoresis, differential centrifugal sedimentation analyses and luminescence spectroscopy. Strikingly, after conjugation with Eu3+ TTA complex, the magnetic nanoparticles show lower adsorption affinity to proteins at higher blood plasma concentration. Moreover, the Eu3+ compound is featured with the narrow emission lines of D-5(0)-> F-7(J) (J=0-4) transitions, imparting additional characteristics to bifunctional nanoparticles that were used as probes to evaluate the protein corona formation.

CHEMNANOMAT 4[12], 1202-1208, 2018. DOI: 10.1002/cnma.201800358

[P479-2018] "Search for a charged Higgs boson decaying to charm and bottom quarks in proton-proton collisions at root s=8TeV"

Sirunyan, A. M.; Tumasyan, A.; **Chinellato, J. A.*; Tonelli Manganote, E. J.***; et al.
CMS Collaboration

A search for charged Higgs boson decaying to a charm and a bottom quark pair production in which one top quark decays to a charged Higgs boson and a bottom quark and the other decays to a charged lepton, a neutrino, and a bottom quark. Charged Higgs boson decays to are searched for, resulting in a final state containing at least four jets, a charged lepton (muon or electron), and missing transverse momentum. A kinematic fit is performed to identify the pair of jets least likely to be the bottom quarks originating from direct top quark decays and the invariant mass of this pair is used as the final observable in the search.

No evidence for the presence of a charged Higgs boson is observed and upper limits at 95% confidence level of 0.8-0.5% are set on the branching fraction B(t H(+)b), assuming B(H+ = 1.0 and B(t H(+)b) + B(t Wb) = 1.0, for the charged Higgs boson mass range 90-150 GeV.

JOURNAL OF HIGH ENERGY PHYSICS 11, 115, 2018. DOI: 10.1007/JHEP11(2018)115

[P480-2018] "Search for a massive resonance decaying to a pair of Higgs bosons in the four b quark final state in proton--proton collisions at root s=13 TeV"

Sirunyan, A. M.; Tumasyan, A.; **Chinellato, J. A.*; Tonelli Manganote, E. J.***; et al.
CMS Collaboration

A search for a massive resonance decaying into a pair of standard model Higgs bosons, in a final state consisting of two b quark-antiquark pairs, is performed. A data sample of proton--proton collisions at a centre-of-mass energy of 13 TeV is used, collected by the CMS experiment at the CERN LHC in 2016, and corresponding to an integrated luminosity of 35.9 fb(-1). The Higgs bosons are highly Lorentz-boosted and are each reconstructed as a single large-area jet. The signal is characterized by a peak in the dijet invariant mass distribution, above a background from the standard model multijet production. The observations are consistent with the background expectations, and are interpreted as upper limits on the products of the s--channel production cross sections and branching fractions of narrow bulk gravitons and radions in warped extra-dimensional models. The limits range from 126 to 1.4 fb at 95% confidence level for resonances with masses between 750 and 3000 GeV, and are the most stringent to date, over the explored mass range.

PHYSICS LETTERS B 781, 244-269, 2018. DOI: 10.1016/j.physletb.2018.03.084

[P481-2018] "Search for heavy resonances decaying into a vector boson and a Higgs boson in final states with charged leptons, neutrinos and b quarks at root s=13 TeV"

Sirunyan, A. M.; Tumasyan, A.; **Chinellato, J. A.*; Tonelli Manganote, E. J.***; et al.
CMS Collaboration

A search for heavy resonances, decaying into the standard model vector bosons and the standard model Higgs boson, is presented. The final states considered contain a b quark-antiquark pair from the decay of the Higgs boson, along with electrons and muons and missing transverse momentum, due to undetected neutrinos, from the decay of the vector bosons. The mass spectra are used to search for a localized excess consistent with a resonant particle. The data sample corresponds to an integrated luminosity of 35.9 fb(-1) collected in 2016 by the CMS experiment at the CERN LHC from proton-proton collisions at a center-of-mass energy of 13 TeV. The data are found to be consistent with background expectations. Exclusion limits are set in the context of spin-0 two Higgs doublet models, some of which include the presence of dark matter. In the spin-1 heavy vector triplet framework, mass-degenerate W and Z resonances with dominant couplings to the standard model gauge bosons are excluded below a mass of 2.9 TeV at 95% confidence level.

JOURNAL OF HIGH ENERGY PHYSICS 11, 172, 2018. DOI: 10.1007/JHEP11(2018)172

[P482-2018] "Search for Leptoquarks Coupled to Third--Generation Quarks in Proton-Proton Collisions at root s=13 TeV"

Sirunyan, A. M.; Tumasyan, A.; **Chinellato, J. A.*; Tonelli Manganote, E. J.***; et al.
CMS Collaboration

Three of the most significant measured deviations from standard model predictions, the enhanced decay rate for B -> D-(*())tau nu, hints of lepton universality violation in B -> K-(*())ll decays, and the anomalous magnetic moment of the muon, can be explained by the existence of leptoquarks (LQs) with large couplings to third-generation quarks and masses at the TeV scale. The existence of these states can be probed at the LHC in high energy proton-proton collisions. A novel search is presented for pair production of LQs coupled to a top quark and a muon using data at a center-of-mass energy of 13 TeV, corresponding to an integrated luminosity of 35.9 fb(-1), recorded by the CMS experiment. No deviation from the standard model prediction has been observed and scalar LQs decaying exclusively into t mu are excluded up to masses of 1420 GeV. The results of this search are combined with those from previous searches for LQ decays into t tau and b nu, which excluded scalar LQs below masses of 900 and 1080 GeV. Vector LQs are excluded up to masses of 1190 GeV for all possible combinations of branching fractions to t mu, t tau and b nu. With this analysis, all relevant couplings of LQs with an electric charge of -1/3 to third-generation quarks are probed for the first time.

PHYSICAL REVIEW LETTERS 121[24], 241802, 2018. DOI: 10.1103/PhysRevLett.121.241802

[P483-2018] "Search for pair-produced resonances decaying to quark pairs in proton-proton collisions at root s=13 TeV"

Sirunyan, A. M.; Tumasyan, A.; **Chinellato, J. A.*; Tonelli Manganote, E. J.***; et al.
CMS Collaboration

A general search for the pair production of resonances, each decaying to two quarks, is reported. The search is conducted separately for heavier resonances (masses above 400 GeV), where each of the four final-state quarks generates a hadronic jet resulting in a four-jet signature, and for lighter resonances (masses between 80 and 400 GeV), where the pair of quarks from each resonance is collimated and reconstructed as a single jet resulting in a two-jet signature. In addition, a b-tagged selection is applied to target resonances with a bottom quark in the final state. The analysis uses data collected with the CMS detector at the CERN LHC, corresponding to an integrated luminosity of 35.9 fb(-1), from proton-proton collisions at a center-of-mass energy of 13 TeV. The mass spectra are analyzed for the presence of new resonances, and are found to be consistent with standard model expectations. The results are interpreted in the framework of R-parity-violating supersymmetry assuming the pair production of scalar top quarks decaying via the hadronic coupling lambda ''(312) or lambda ''(323) and upper limits on the cross section as a function of the top squark mass are set. These results probe a wider range of masses than previously explored at the LHC, and extend the top squark mass limits in the (t) over tilde -> qq' scenario.

PHYSICAL REVIEW D 98[11], 112014, 2018. DOI: 10.1103/PhysRevD.98.112014

[P484-2018] "Search for resonances in the mass spectrum of muon pairs produced in association with b quark jets in proton-proton collisions at root 8 and 13 TeV"

Sirunyan, A. M.; Tumasyan, A.; **Chinellato, J. A.*; Tonelli Manganote, E. J.***; et al.
CMS Collaboration

A search for resonances in the mass range 12-70 GeV produced in association with a b quark jet and a second jet, and decaying to a muon pair, is reported. The analysis is based on data from proton-proton collisions at center-of-mass energies of 8 and 13 TeV, collected with the CMS detector at the LHC and corresponding to integrated luminosities of 19.7 and 35.9 fb(-1), respectively. The search is carried out in two mutually exclusive event categories. Events in the first category are required to have a b quark jet in the central region (|| 2.4) and at least one jet in the forward region (|| > 2.4). Events in the second category are required to have two jets in the central region, at least one of which is identified as a b quark jet, no jets in the forward region, and low missing transverse momentum. An excess of events above the background near a dimuon mass of 28 GeV is observed in the 8 TeV data, corresponding to local significances of 4.2 and 2.9 standard deviations for the first and second event categories, respectively. A similar analysis conducted with the 13 TeV data results in a mild excess over the background in the first event category corresponding to a local significance of 2.0 standard deviations, while the second category results in a 1.4 standard deviation deficit. The fiducial cross section measurements and 95% confidence level upper limits on those for a resonance consistent with the 8 TeV excess are provided at both collision energies.

JOURNAL OF HIGH ENERGY PHYSICS 11, 161, 2018. DOI: 10.1007/JHEP11(2018)161

[P485-2018] "Searches for pair production of charginos and top squarks in final states with two oppositely charged leptons in proton-proton collisions at root s=13 TeV"

Sirunyan, A. M.; Tumasyan, A.; **Chinellato, J. A.*; Tonelli Manganote, E. J.***; et al.
CMS Collaboration

A search for pair production of supersymmetric particles in events with two oppositely charged leptons (electrons or muons) and missing transverse momentum is reported. The data sample corresponds to an integrated luminosity of 35.9 fb(-1) of proton-proton collisions at TeV collected with the CMS detector during the 2016 data taking period at the LHC. No significant deviation is observed from the predicted standard model background. The results are interpreted in terms of several simplified models for chargino and top squark pair production, assuming R-parity conservation and with the neutralino as the lightest supersymmetric particle. When the chargino is assumed to undergo a cascade decay through sleptons, with a slepton mass equal to the average of the chargino and neutralino masses, exclusion limits at 95% confidence level are set on the masses of the chargino and neutralino up to 800 and 320 GeV, respectively. For top squark pair production, the search focuses on models with a small mass difference between the top squark and the lightest neutralino. When the top squark decays into an off-shell top quark and a neutralino, the limits extend up to 420 and 360 GeV for the top squark and neutralino masses, respectively.

JOURNAL OF HIGH ENERGY PHYSICS 11, 079, 2018. DOI: 10.1007/JHEP11(2018)079

[P486-2018] "Star-galaxy classification in the Dark Energy Survey Y1 data set"

Sevilla-Noarbe, I.; Hoyle, B.; **Sobreira, F.***; et.al.
DES Collaboration;

We perform a comparison of different approaches to star--galaxy classification using the broadband photometric data from Year 1 of the Dark Energy Survey. This is done by performing a wide range of tests with and without external 'truth' information, which can be ported to other similar data sets. We make a broad evaluation of the performance of the classifiers in two science cases with DES data that are most affected by this systematic effect: large-scale structure and Milky Way studies. In general, even though the default morphological classifiers used for DES Y1 cosmology studies are sufficient to maintain a low level of systematic contamination from stellar misclassification, contamination can be reduced to the O(1 per cent) level by using multi-epoch and infrared information from external data sets. For Milky Way studies, the stellar sample can be augmented by similar to 20 per cent for a given flux limit.

MONTHLY NOTICES OF THE ROYAL ASTRONOMICAL SOCIETY 481[4] 5451-5469, 2018. DOI: 10.1093/mnras/sty2579

[P487-2018] "Structural analysis of magnetic nanocomposites based on chitosan"

Kloster, G. A.; **Muraca, D.*; Londono, O. M.*; Knobel, M.***; Marcovich, N. E.; Mosiewicki, M. A.

This work investigates the structure and magnetic properties of chitosan based films with different contents of magnetic nanoparticles (MNPs) of around 10 nm as well as the effects of the addition of glycerol as plasticizer. Synthesized MNPs were dispersed in the chitosan film forming solution by ultrasonication and then composite films were obtained by casting. From the morphological analysis, a bimodal distribution of clusters was detected; the larger ones seem to be present mostly in the plasticized samples. Regarding the mechanical behavior of the samples, for the non-plasticized samples the outstanding increase in modulus and strength with the increasing content of MNP was explained by a strong interfacial adhesion and very good particles dispersion into the chitosan matrix. This fact was also supported by the model applyed to the strength as a function of the volume fraction of MNP. Regarding magnetic properties, all nanocomposite films evidenced systems with particles of strong dipolar interactions that lead to blocking and irreversibility temperatures close to room temperature (RT). Even though the isothermal magnetization results showed that the particles in the nanocomposite films behave as super paramagnetic at the highest analyzed temperature (RT). Langevin model as well as FESEM and SAXS analysis supported the hypothesis that the formation of aggregates with different features dominates the magnetic response through collective behavior, mainly in the plasticized films.

POLYMER TESTING 72, 202-213, 2018. DOI: 10.1016/j.polymertesting.2018.10.022

[P488-2018] "Studies of B-s2*(5840)(0) and B-s1(5830)(0) mesons including the observation of the B-s2*(5840)(0) -> (BKS0)-K-0 decay in proton- proton collisions at root s=8 TeV"

Sirunyan, A. M.; Tumasyan, A.; **Chinellato, J. A.*; Tonelli Manganote, E. J.***; et al.
CMS Collaboration

Measurements of B-s2*(5840)(0) and B-s1(5830)(0) mesons are performed using a data sample of proton-proton collisions corresponding to an integrated luminosity of 19.6 fb(-1), collected with the CMS detector at the LHC at a centre--of-mass energy of 8 TeV. The analysis studies P-wave B-s(0) meson decays into B(*)(+)K(-)and B(*)K-0(S)0, where the B+ and B-0 mesons are identified using the decays B+ -> J/psi K+ and B-0 -> J/psi K* (892)(0). The masses of the P-wave B-s(0) meson states are measured and the natural width of the B-s2*(5840)(0) state is determined. The first measurement of the mass difference between the charged and neutral B* mesons is also presented. The B-s2*(5840)(0) decay to (BKS0)-K-0 is observed, together with a measurement of its branching fraction relative to the B-s2*(5840)(0) -> B+K- decay.

EUROPEAN PHYSICAL JOURNAL C 78[11], 939, 2018. DOI: 10.1140/epjc/s10052-018-6390-z

[P489-2018] "Switching the Spin-Crossover Phenomenon by Ligand Design on Imidazole-Diazineiron(II) Complexes"

Bibi, N.; Ratier de Arruda, E. G.; Domingo, A.; Oliveira, A. A.; Galuppo, C.; Phung, Q. M. P.; Orra, N. M.; **Beron, F.***; Paesano, A.; Pierloot, K.; Formiga, A. L. B.

The iron(II) complexes of two structural isomers of 2-(1H-imidazol-2-yl)diazine reveal how ligand design can be a successful strategy to control the electronic and magnetic properties of complexes by fine-tuning their ligand field. The two isomers only differ in the position of a single diazinic nitrogen atom, having either a pyrazine (Z) or a pyrimidine (M) moiety. However, [Fe(M)(3)](ClO4)(2) is a spin-crossover complex with a spin transition at 241 K, whereas [Fe(Z)(3)](ClO4)(2) has a stable magnetic behavior between 2 and 300 K. This is corroborated by temperature-dependent Mossbauer spectra showing the presence of a quintet and a singlet state in equilibrium. The temperature-dependent single crystal X-ray diffraction results relate the spin-crossover observed in [Fe(M)(3)](ClO4)(2) to changes in the bond distances and angles of the coordination sphere of iron(II), hinting at a stronger sigma donation of ligand Z in comparison to ligand M. The UV/vis spectra of both complexes are solved by means of the multiconfigurational wave-function-based method CASPT2 and confirm their different spin multiplicities at room temperature, as observed in the Mossbauer spectra. Calculations show larger stabilization of the singlet state in [Fe(Z)(3)](2+) than in [Fe(M)(3)](2+), stemming from the slightly stronger ligand field of the former (506 cm(-1) in the singlet). This relatively weak effect is indeed capable of changing the spin multiplicity of the complexes and causes the appearance of the spin transition in the M complex.

INORGANIC CHEMISTRY 57[23] 14603-14616, 2018. DOI: 10.1021/acs.inorgchem.8b02278

[P490-2018] "Wettability, Photoactivity, and Antimicrobial Activity of Glazed Ceramic Tiles Coated with Titania Films Containing Tungsten"

Onna, D.; Fuentes, K. M.; Spedalieri, C.; Perullini, M.; Marchi, M. C.; **Alvarez, F.***; Candal, R. J.; Bilmes, S. A.

Self-cleaning coatings are advanced materials for the removal of pollutants and microorganisms by combining wettability, photocatalytic degradation, and antimicrobial activity. In this work, we propose a rational design of self-cleaning films based on TiO2 synthesized by sol-gel on commercial glazed ceramic tiles for building's indoor applications. The synthesis strategy is based on hydrolysis and condensation of Ti-isopropoxide in the presence of W(VI) precursors to tune defects and crystallinity of the resulting W-TiO2 thin film. From the microstructure and surface composition analysis for different tungsten contents and annealing temperatures, we conclude that the film is composed by sintered TiO2 particles with adsorbed polytungstates (WOx) that inhibit anatase/rutile transformation. Polytungstates on TiO2 also induce surface defects that enhance water contact angle and inactivation of Escherichia coli under visible light. The presence of W(VI) has a negligible effect toward crystal violet degradation either under visible or under UV light. These results provide evidence on the existence of at least two different types of defects: (i) intrinsic defect from a sol-gel route and (ii) induced defect by tungsten species on the surface. Understanding the correlation between composition, structure, and self-cleaning properties provides a base for an efficient design of low-cost self-cleaning ceramic tiles that can be fully manufactured in an industrial plant.

ACS OMEGA 3[12], 17629-17636, 2018. DOI: 10.1021/acsomega.8b03339

[P491-2018] "Noninvasive continuous optical monitoring of absolute cerebral blood flow in critically ill adults"

He, L.; Baker, W. B.; Milei, D.; Kavuri, V. C.; **Mesquita, R. C.***; Busch, D. R.; Abramson, K.; Jiang, J. Y.; Diop, M.; St Lawrence, K.; Amendolia, O.; Quattrone, F.; Balu, R.; Kofke, W. A.; Yodh, A. G.

We investigate a scheme for noninvasive continuous monitoring of absolute cerebral blood flow (CBF) in adult human patients based on a combination of time-resolved dynamic contrast--enhanced near-infrared spectroscopy (DCE-NIRS) and diffuse correlation spectroscopy (DCS) with semi-infinite head model of photon propogation. Continuous CBF is obtained via calibration of the DCS blood flow index (BFI) with absolute CBF obtained by intermittent intravenous injections of the optical contrast agent indocyanine green. A calibration coefficient (gamma) for the CBF is thus determined, permitting conversion of DCS BFI to absolute blood flow units at all other times. A study of patients with acute brain injury (N = 7) is carried out to ascertain the stability of gamma. The patient-averaged DCS calibration coefficient across multiple monitoring days and multiple patients was determined, and good agreement between the two calibration coefficients measured at different times during single monitoring days was found. The patient-averaged calibration coefficient of 1.24 x 10(9) (mL/100 g/min)/(cm(2)/s) was applied to previously measured DCS BFI from similar brain--injured patients; in this case, absolute CBF was underestimated compared with XeCT, an effect we show is primarily due to use of semi-infinite homogeneous models of the head.

NEUROPHOTONICS 5[4], 045006, 2018. DOI: 10.1117/1.NPh.5.4.045006

Eventos publicados 2018

[P492-2018] "Nonlinear Spectroscopy in Perovskite Quantum Dots"

Nagamine, G.*; Bonato, L. G.; **Castaneda, J. A.***; Yassitepe, E.; Nogueira, A. F.; **Cruz, C. H. B.*; Padilha, L. A.***

Since the first reports of their successful synthesis in 2015, all-inorganic perovskite quantum dots (PQDs), emerged as promising material for lighting applications. Despite their unique optical properties, to date, PQDs based LEDs and lasing media operation is still far from ideal. One of the limiting factors is the strong Coulomb interaction, which contributes to nonradiative decay processes. Here, we discuss in detail the multiexciton interactions in PQDs based on their size dependence. We expand on their nonlinear optical properties, focusing on the two-photon absorption characteristics, showing results for two-photon pumped amplified stimulated emission, suggesting that these materials may be promising for two-photon pumped lasers.

ULTRAFAST BANDGAP PHOTONICS III, Proceedings of SPIE 10638, UNSP 106380K, 218. DOI: 10.1117/12.2305001

Conference on Ultrafast Bandgap Photonics III. Orlando, FL. APR 16-19, SPIE. 2018.

[P493-2018] "Squeeze operators in classical and quantum scenarios"

Anaya-Contreras, J. A.; Zuniga-Segundo, A.; Soto-Eguibar, F.; Arrizon, V.; **Vidiella-Barranco, A.***; Moya-Cessa, H. M.

We show how squeeze operators appear in paraxial field propagation,i.e., in classical optics. Then, we show how squeezed states may be generated in multiphoton processes that occur in single photon resonant transitions of the atom-field interaction when conditional measurements take place. We study field properties, to show that the field does not only acquire squeezed properties but also can gain or lose more than one photon.

QUANTUM COMMUNICATIONS AND QUANTUM IMAGING XVI, Proceedings of SPIE, 10771, UNSP 107710Y, 2018. DOI: 10.1117/12.2317991

Conference on Quantum Communications and Quantum Imaging XVI. San Diego, CA. AUG 19-20, SPIE. 2018.

[P494-2018] "X-ray coherent diffraction imaging: Sequential inverse problems simulation"

Rinkel, J.*; Polli, J. M.; Miqueles, E. X.

Improvement of spatial coherence in third generation synchrotron beamlines made possible the development of X-ray plane-wave coherent diffraction imaging technique (plane-wave CDI), which enables 3D imaging at nanometric resolution. In this work, we first simulated the influence of detector geometry by comparing reconstruction quality of planar samples made of gold nanoparticles. We compared a commercially available detector geometry with the next Medipix3-based large area detector designed for the next fourth generation Brazilian synchrotron, sirius. The spatial resolution was highly improved, from 7.2 nm for the commercial geometry to 4.8 nm for the Medipix3 detector by keeping the same global image quality. Finally, global image qualities were compared by adjusting the sample-to-detectors distances at a given spatial resolution. For thick samples reconstruction at such high nanometric resolutions, the main limitation of current reconstruction approaches are due to the complex wave propagation within the sample, given by the inhomogeneous Helmholtz equation. We proposed an iterative method to reconstruct the complex refraction index. This method enables to keep the image quality almost constant beyond the resolution limit for thick samples made of gold nanoparticles in water.

NUCLEAR INSTRUMENTS & METHODS IN PHYSICS RESEARCH SECTION A-ACCELERATORS SPECTROMETERS DETECTORS AND ASSOCIATED EQUIPMENT 912[SI], 43-47, 2018. DOI: 10.1016/j.nima.2017.10.032

8th International Conference on New Developments in Photodetection (NDIP). Tours, FRANCE. JUL, 2017.

Artigos publicados 2019

[P001-2019] "Accurate pi/2-phase shifting setup for a stabilized interference pattern of light fringes"

de Oliveira, I.; Bertasso, F. B.; Georges, M.; **Frejlich, J.***

We report on a technique for accurately pi/2-phase shifting a stabilized interference pattern of light fringes used for building up a map of phase for 2D deformation measurement. This technique is based on the use of low amplitude phase modulation on the setup in order to generate first and second harmonics temporal terms in the pattern of light to operate an actively stabilized setup. Particular features of this stabilization setup allow one to use them for accurate pi/2-phase shifting with the practical advantage of operating on an already stabilized pattern of fringes.

OPTIK 178, 879-883, 2019. DOI: 10.1016/j.ijleo.2018.10.090

[P002-2019] "Dark Energy Survey year 1 results: galaxy sample for BAO measurement"

Crocce, M.; Ross, A. J.; **Sobreira, F.***; et. al.;
Dark Energy Survey Collaboration

We define and characterize a sample of 1.3million galaxies extracted from the first year of Dark Energy Survey data, optimized to measure baryon acoustic oscillations (BAO) in the presence of significant redshift uncertainties. The sample is dominated by luminous red galaxies located at redshifts z greater than or similar to 0.6. We define the exact selection using colour and magnitude cuts that balance the need of high number densities and small photometric redshift uncertainties, using the corresponding forecasted BAO distance error as a figure-of-merit in the process. The typical photo z uncertainty varies from 2.3 per cent to 3.6 per cent (in units of 1+z) from z = 0.6 to 1, with number densities from 200 to 130 galaxies per deg(2) in tomographic bins of width Delta z = 0.1. Next, we summarize the validation of the photometric redshift estimation. We characterize and mitigate observational systematics including stellar contamination and show that the clustering on large scales is robust in front of those contaminants. We show that the clustering signal in the autocorrelations and cross--correlations is generally consistent with theoretical models, which serve as an additional test of the redshift distributions.

MONTHLY NOTICES OF THE ROYAL ASTRONOMICAL SOCIETY 482 [2], 2807-2822, 2019. DOI: 10.1093/mnras/sty2522

[P003-2019] "Dark Energy Survey Year 1 results: Methodology and projections for joint analysis of galaxy clustering, galaxy lensing, and CMB lensing two-point functions"

Baxter, E. J.; Omori, Y.; **Sobreira, F.***; et. al.;
DES Collaboration; SPT Collaboration

Optical imaging surveys measure both the galaxy density and the gravitational lensing-induced shear fields across the sky. Recently, the Dark Energy Survey (DES) Collaboration used a joint fit to two-point correlations between these observables to place tight constraints on cosmology (T. M. C. Abbott et al. (Dark Energy Survey Collaboration), Phys. Rev. D 98, 043526 (2018)). In this work, we develop the methodology to extend the DES Year 1 joint probes analysis to include cross-correlations of the optical survey observables with gravitational lensing of the cosmic microwave background as measured by the South Pole Telescope (SPT) and Planck. Using simulated analyses, we show how the resulting set of five two-point functions increases the robustness of the cosmological constraints to systematic errors in galaxy lensing shear calibration. Additionally, we show that contamination of the SPT+Planck cosmic microwave background lensing map by the thermal Sunyaev-Zel'dovich effect is a potentially large source of systematic error for two-point function analyses but show that it can be reduced to acceptable levels in our analysis by masking clusters of galaxies and imposing angular scale cuts on the two-point functions. The methodology developed here will be applied to the analysis of data from the DES, the SPT, and Planck in a companion work.

PHYSICAL REVIEW D 99[2], 023508, 2019. DOI: 10.1103/PhysRevD.99.023508

[P004-2019] "Dark Energy Survey Year 1 results: weak lensing mass calibration of redMaPPer galaxy clusters"

McClintock, T.; Varga, T. N.; **Sobreira, F.***; et. al.;
DES Collaboration

We constrain the mass-richness scaling relation of redMaPPer galaxy clusters identified in the Dark Energy Survey Year 1 data using weak gravitational lensing.

We split clusters into 4 x 3 bins of richness lambda and redshift z for lambda >= 20 and 0.2 <= z <= 0.65 and measure the mean masses of these bins using their stacked weak lensing signal. By modelling the scaling relation as M-200m|lambda, M-0(lambda/40)(F)((1 + /1.35)(G), we constrain the normalization of the scaling relation at the 5.0 per cent level, finding M-0 = [3.081 +/- 0.075(stat) +/- 0.133(sys)] center dot 10(14) M-aS (TM) at lambda = 40 and = 0.35. The recovered richness scaling index is F = 1.356 +/- 0.051 (stat) +/- 0.008 (sys) and the redshift scaling index G = -0.30 +/- 0.30 (stat) +/- 0.06 (sys). These are the tightest measurements of the normalization and richness scaling index made to date from a weak lensing experiment. We use a semi-analytic covariance matrix to characterize the statistical errors in the recovered weak lensing profiles. Our analysis accounts for the following sources of systematic error: shear and photometric redshift errors, cluster miscentring, cluster member dilution of the source sample, systematic uncertainties in the modelling of the halo-mass correlation function, halo triaxiality, and projection effects. We discuss prospects for reducing our systematic error budget, which dominates the uncertainty on M-0. Our result is in excellent agreement with, but has significantly smaller uncertainties than, previous measurements in the literature, and augurs well for the power of the DES cluster survey as a tool for precision cosmology and upcoming galaxy surveys such as LSST, Euclid, and WFIRST.

MONTHLY NOTICES OF THE ROYAL ASTRONOMICAL SOCIETY 482[1], 1352-1378, 2019. DOI: 10.1093/mnras/sty2711

[P005-2019] "DFT and canonical ensemble investigations on the thermodynamic properties of Syngas and natural gas/ Syngas mixtures"

Neto, A. F. G.; **Marques, F. C.***; Amador, A. T.; Ferreira, A. D. S.; Neto, A. M. J. C.

Density Functional Theory and canonical ensemble were used to investigate thermodynamic properties of Syngas and its mixture with natural gas. The following thermodynamic potentials were obtained: internal energy, enthalpy, entropy and Gibbs free energy for temperatures ranging from 0.5 K to 1500 K. It was observed that CO and H-2 were the most stable Syngas components, possessing the ability to render Syngas less favorable to the temperature increase. Also, we verified that Syngas presents properties similar to an antiknock agent for natural gas, raising its resistance to temperature increases. Were determined the Poisson coefficients and Bulk modulus for Natural gas/Syngas mixtures and Shomate equation coefficients for some Syngas types, providing a more complete thermodynamic description for these gases. Additionally, thermodynamic potentials of combustion for Natural gas/Syngas mixtures were predicted, showing that this biofuel can reduce the calorific power of natural gas and makes its combustion less favorable due its antiknock behavior. However, a mixture with 30% of Syngas may be useful for natural gas combustion, since it present a calorific power between 73.41% and 79.49% of that of natural gas, which is a substantial fraction of energy released during combustion, showing good future prospects to the Natural gas/Syngas mixture to the renewable energy generation.

RENEWABLE ENERGY 130, 495-509, 2019. DOI: 10.1016/j.renene.2018.06.091

[P006-2019] "Dielectron and heavy-quark production in inelastic and high-multiplicity proton-proton collisions at root s=13 TeV"

Acharya, S.; Acosta, F. T.; **Albuquerque, D. S. D.*; Chinellato, D. D.*; De Souza, R. D.*; Takahashi, J.*;** et. al.
ALICE Collaboration

The measurement of dielectron production is presented as a function of invariant mass and transverse momentum (p(T)) at midrapidity (vertical bar ye vertical bar < 0.8) in proton--proton (pp) collisions at a centre-of-mass energy of root s = 13 TeV. The contributions from light-hadron decays are calculated from their measured cross sections in pp collisions at root s = 7 TeV or 13 TeV. The remaining continuum stems from correlated semileptonic decays of heavy-flavour hadrons. Fitting the data with templates from two different MC event generators, PYTHIA and POWHEG, the charm and beauty cross sections at midrapidity are extracted for the first time at this collision energy: d sigma(c<(c)over bar>)/dy vertical bar(y=0) = 974 +/- 138 (stat.) +/- 140 (syst.) +/- 214(BR) mu b and d sigma(b (b) over bar)/dy vertical bar(y=0) = 79 +/- 14 (stat.) +/- 11 (syst.) +/- 5(BR) mu b using PYTHIA simulations and d sigma(c (c) over bar)/dy vertical bar(y=0) = 1417 +/- 184 (stat.) +/- 204 (syst.) +/- 312(BR) mu b and d sigma(b (b) over bar)/dy vertical bar(y=0) = 48 +/- 14 (stat.) +/- 7 (syst.) +/- 3(BR) mu b for POWHEG. These values, whose uncertainties are fully correlated between the two generators, are consistent with extrapolations from lower energies. The different results obtained with POWHEG and PYTHIA imply different kinematic correlations of the heavy-quark pairs in these two generators. Furthermore, comparisons of dielectron spectra in inelastic events and in events collected with a trigger on high charged-particle multiplicities are presented in various p(T) intervals. The differences are consistent with the already measured scaling of light-hadron and open-charm production at high charged-particle multiplicity as a function of p(T). Upper limits for the contribution of virtual direct photons are extracted at 90% confidence level and found to be in agreement with pQCD calculations.

PHYSICS LETTERS B 788, 505-518, 2019. DOI: 10.1016/j.physletb.2018.11.009

[P007-2019] "Global synchronization of partially forced Kuramoto oscillators on networks"

Moreira, C. A.*; de Aguiar, M. A. M.*

We study the synchronization of Kuramoto oscillators on networks where only a fraction of them is subjected to a periodic external force. When all oscillators receive the external drive the system always synchronize with the periodic force if its intensity is sufficiently large. Our goal is to understand the conditions for global synchronization as a function of the fraction of nodes being forced and how these conditions depend on network topology, strength of internal couplings and intensity of external forcing. Numerical simulations show that the force required to synchronize the network with the external drive increases as the inverse of the fraction of forced nodes. However, for a given coupling strength, synchronization does not occur below a critical fraction, no matter how large is the force. Network topology and properties of the forced nodes also affect the critical force for synchronization. We develop analytical calculations for the critical force for synchronization as a function of the fraction of forced oscillators and for the critical fraction as a function of coupling strength. We also describe the transition from synchronization with the external drive to spontaneous synchronization.

PHYSICA A-STATISTICAL MECHANICS AND ITS APPLICATIONS 514, 487-496, 2019. DOI: 10.1016/j.physa.2018.09.096

[P008-2019] "High temperature quasistatic and dynamic mechanical behavior of interconnected 3D carbon nanotube structures"

Bhowmick, S.; Ozden, S.; Bizao, R. A.; Machado, L. D.; Asif, S. A. S.; Pugno, N. M.; **Galvao, D. S.***; Tiwary, C. S.; Ajayan, P. M.

Carbon nanotubes (CNTs) are one of the most appealing materials in recent history for both research and commercial interest because of their outstanding physical, chemical, and electrical properties. This is particularly true for 3D arrangements of CNTs which enable their use in larger scale devices and structures. In this paper, the effect of temperature on the quasistatic and dynamic deformation behavior of 3D CNT structures is presented for the first time. An in situ high-temperature nanomechanical instrument was used inside an SEM at high vacuum to investigate mechanical properties of covalently interconnected CNT porous structures in a wide range of temperature. An irreversible bucking at the base of pillar samples was found as a major mode of deformation at room and elevated temperatures. It has been observed that elastic modulus and critical load to first buckle formation decrease progressively with increasing temperature from 25 degrees C to 750 degrees C. To understand fatigue resistance, pillars made from this unique structure were compressed to 100 cycles at room temperature and 750 degrees C. While the structure showed remarkable resistance to fatigue at room temperature, high temperature significantly lowers fatigue resistance. Molecular dynamics (MD) simulation of compression highlights the critical role played by covalent interconnections which prevent localized bending and improve mechanical properties.

CARBON 142, 291-299, 2019. DOI: 10.1016/j.carbon.2018.09.075

[P009-2019] "Lie point symmetries and conservation laws for a class of BBM-KdV systems"

Silva, V. A.*

We determine the Lie point symmetries of a class of BBM--KdV systems and establish its nonlinear self-adjointness. We then construct conservation laws via Ibragimov's Theorem.

COMMUNICATIONS IN NONLINEAR SCIENCE AND NUMERICAL SIMULATION 69, 73-77, 2019. DOI: 10.1016/j.cnsns.2018.09.011

[P010-2019] "Measurement of differential cross sections for inclusive isolated-photon and photon plus jet production in proton-proton collisions at root s=13TeV"

Sirunyan, A. M.; Tumasyan, A.; **Chinellato, J. A.*; Tonelli Manganote, E. J.***; et al.
CMS Collaboration

Measurements of inclusive isolated-photon and photon+jet production in proton-proton collisions at =13TeV are presented. The analysis uses data collected by the CMS experiment in 2015, corresponding to an integrated luminosity of 2.26fb-1. The cross section for inclusive isolated photon production is measured as a function of the photon transverse energy in a fiducial region. The cross section for photon+jet production is measured as a function of the photon transverse energy in the same fiducial region with identical photon requirements and with the highest transverse momentum jet. All measurements are in agreement with predictions from next-to-leading-order perturbative QCD.

EUROPEAN PHYSICAL JOURNAL C 79[1], 20, 2019. DOI: 10.1140/epjc/s10052-018-6482-9

[P011-2019] "Measuring linear and non-linear galaxy bias using counts-in-cells in the Dark Energy Survey Science Verification data"

Salvador, A. I.; Sanchez, F. J.; **Sobreira, F.***; et. al.
DES Collaboration

Non-linear bias measurements require a great level of control of potential systematic effects in galaxy redshift surveys. Our goal is to demonstrate the viability of using counts-in-cells (CiC), a statistical measure of the galaxy distribution, as a competitive method to determine linear and higher-order galaxy bias and assess clustering systematics. We measure the galaxy bias by comparing the first four moments of the galaxy density distribution with those of the dark matter distribution. We use data from the MICE simulation to evaluate the performance of this method, and subsequently perform measurements on the public Science Verification data from the Dark Energy Survey. We find that the linear bias obtained with CiC is consistent with measurements of the bias performed using galaxy-galaxy clustering, galaxy-galaxy lensing, cosmic microwave background lensing, and shear + clustering measurements. Furthermore, we compute the projected (2D) non-linear bias using the expansion delta(g) = Sigma(3)(k=0)(b(k)/k!) delta(k), finding a non-zero value for b(2) at the 3 sigma level. We also check a non-local bias model and show that the linear bias measurements are robust to the addition of new parameters. We compare our 2D results to the 3D prediction and find compatibility in the large-scale regime (>30 h(-1) Mpc).

MONTHLY NOTICES OF THE ROYAL ASTRONOMICAL SOCIETY 482[2], 435-1451, 2019. DOI: 10.1093/mnras/sty2802

[P012-2019] "Pressure effects on the structural and superconducting transitions in La3Co4Sn13"

Mendonca-Ferreira, L.; Carneiro, F. B.; Fontes, M. B.; Baggio--Saitovitch, E.; Veiga, L. S., I; Mardegan, J. R. L.; Strempfer, J.; **Piva, M. M.*; Pagliuso, P. G.*;** dos Reis, R. D.; Bittar, E. M.

La3Co4Sn13 is a superconducting material with transition temperature at T-c = 2.70 K, which presents a superlattice structural transition at T* similar or equal to 150 K, a common feature for this class of compounds. However, for this material, it is not clear that at T' the lattice distortions arise from a charge density wave (CDW) or from a distinct microscopic origin. Interestingly, it has been suggested in isostructural non-magnetic intermetallic compounds that T* can be suppressed to zero temperature, by combining chemical and external pressure, and a quantum critical point is argued to be observed near these critical doping/pressure. Our study shows that application of pressure on single-crystalline La-3Co4Sn13 enhances T-c and decreases T*. We observe thermal hysteresis loops for cooling/heating cycles around T* for P greater than or similar to 0.6 GPa, in electrical resistivity measurements, which are not seen in x-ray diffraction data. The hysteresis in electrical measurements may be due to the pinning of the CDW phase to impurities/defects, while the superlattice structural transition maintains its ambient pressure second-order transition nature under pressure. From our experiments we estimate that T* vanishes at around 5.5 GPa, though no quantum critical behavior is observed up to 2.53 GPa.

JOURNAL OF ALLOYS AND COMPOUNDS 773, 34-39, 2019. DOI: 10.1016/j.jallcom.2018.09.236

[P013-2019] "Relativistic Proton Levels from Region AR 12673 (GLE #72) and the Heliospheric Current Sheet as a Sun-Earth Magnetic Connection"

Augusto, C. R. A.; Navia, C. E.; de Oliveira, M. N.; Nepomuceno, A. A.; **Fauth, A. C.*;** Kopenkin, V.; Sinzi, T.

On 2017 September 10 Neutron Monitors (NMs) apparatus located at ground level and high latitudes detected an increase in the counting rate associated to solar energetic particles (SEPs) emission from X8.2-class solar flare and its associated CME. This was the second-highest flare of the current solar cycle.

The origin was the active region AR 12673 when it was located at the edge of the west solar disk, magnetically poorly connected with Earth. However, there was a peculiar condition: the solar protons accelerated by the CME shocks were injected within a heliospheric current sheet (HCS) region when Earth was crossing this region. We show that often HCS and SEPs propagation are closely related. If the source locations of SEPs are within or close to HCS, the HCS play the role of a Sun-Earth magnetic connection. SEPs drift around HCS paths, and SEPs are also drift in a wide range of longitudes by the HCSs. In some cases, and especially when Earth crosses the HCS sector, a fraction of these particles can reach Earth with a harder energetic particle flux, triggering a ground-level enhancement (GLE). The blast on 2017 September 10, which triggered the GLE #72, was the second in the current solar cycle. We show that the two GLEs, including all sub-GLEs observed in the current solar cycle, comes from solar explosions that happened within an HCS structure; this behavior is also observed in the GLEs of the previous solar cycle. In general, solar explosions from active regions poorly connected with Earth can trigger GLEs, through the mechanism described above. In all cases, the SEPs drift processes by HCS structures provides an efficient particle transport, allowing the observation of these solar transient events.

PUBLICATIONS OF THE ASTRONOMICAL SOCIETY OF THE PACIFIC 131[996], 024401, 2019 DOI: 10.1088/1538-3873/aaeb7f

[P014-2019] "Search for Higgs boson pair production in the gamma gamma b(b)over-bar final state in pp collisions at root s=13 TeV"

Sirunyan, A. M.; Tumasyan, A.; **Chinellato, J. A.*; Tonelli Manganote, E. J.***; et al.
CMS Collaboration

A search is presented for the production of a pair of Higgs bosons, where one decays into two photons and the other one into a bottom quark-antiquark pair. The analysis is performed using proton-proton collision data at root s = 13 TeV recorded in 2016 by the CMS detector at the LHC, corresponding to an integrated luminosity of 35.9 fb(-1) . The results are in agreement with standard model (SM) predictions. In a search for resonant production, upper limits are set on the cross section for new spin-0 or spin-2 particles. For the SM-like nonresonant production hypothesis, the data exclude a product of cross section and branching fraction larger than 2.0 fb at 95% confidence level (CL), corresponding to about 24 times the SM prediction. Values of the effective Higgs boson self-coupling K X are constrained to be within the range -11 < K-lambda < 17 at 95% CL, assuming all other Higgs boson couplings are at their SM value. The constraints on K-lambda, are the most restrictive to date.

PHYSICS LETTERS B 788, 7-36, 2019. DOI: 10.1016/j.physletb.2018.10.056

[P015-2019] "Search for low-mass resonances decaying into bottom quark-antiquark pairs in proton-proton collisions at root s=13 TeV"

Sirunyan, A. M.; Tumasyan, A.; **Chinellato, J. A.*; Tonelli Manganote, E. J.***; et al.
CMS Collaboration

A search for narrow, low-mass, scalar, and pseudoscalar resonances decaying to bottom quark-antiquark pairs is presented. The search is based on events recorded in root s = 13 TeV proton-proton collisions with the CMS detector at the LHC, collected in 2016, and corresponding to an integrated luminosity of 35.9 fb(-1). The search selects events in which the resonance would be produced with high transverse momentum because of the presence of initial- or final-state radiation. In such events, the decay products of the resonance would be reconstructed as a single large-radius jet with high mass and two-prong substructure. A potential signal would be identified as a narrow excess in the jet invariant mass spectrum. No evidence for such a resonance is observed within the mass range from 50 to 350 GeV, and upper limits at 95% confidence level are set on the product of the cross section and branching fraction to a bottom quark-antiquark pair. These constitute the first constraints from the LHC on exotic bottom quark-antiquark resonances with masses below 325 GeV.

PHYSICAL REVIEW D 99[1], 012005, 2019. DOI: 10.1103/PhysRevD.99.012005

[P016-2019] "Search for the Higgs Boson Decaying to Two Muons in Proton-Proton Collisions at root s=13 TeV"

Sirunyan, A. M.; Tumasyan, A.; **Chinellato, J. A.*; Tonelli Manganote, E. J.***; et al.
CMS Collaboration

A search for the Higgs boson decaying to two oppositely charged muons is presented using data recorded by the CMS experiment at the CERN LHC in 2016 at a center-of-mass energy root s = 13 TeV, corresponding to an integrated luminosity of 35.9 fb(-1). Data are found to be compatible with the predicted background. For a Higgs boson with a mass of 125.09 GeV, the 95% confidence level observed (background-only expected) upper limit on the production cross section times the branching fraction to a pair of muons is found to be 3.0 (2.5) times the standard model expectation. In combination with data recorded at center-of-mass energies root s = 7 and 8 TeV, the background--only expected upper limit improves to 2.2 times the standard model value with a standard model expected significance of 1.0 standard deviation. The corresponding observed upper limit is 2.9 with an observed significance of 0.9 standard deviation. This corresponds to an observed upper limit on the standard model Higgs boson branching fraction to muons of 6.4 x 10(-4) and to an observed signal strength of 1.0 +/- 1.0(stat) +/- 0.1(syst).

PHYSICAL REVIEW LETTERS 122[2], 021801, 2019. DOI: 10.1103/PhysRevLett.122.021801

[P017-2019] "Simultaneous detection of humidity and temperature through an adhesive based Fabry-Perot cavity combined with polymer fiber Bragg grating"

Oliveira, R.; Bilro, L.; **Marques, T. H. R.*; Cordeiro, C. M. B.***; Nogueira, R.

In this work we report the fabrication of a dual fiber sensor composed of an adhesive based Fabry-Perot cavity combined with a polymer fiber Bragg grating (PFBG), for the simultaneous detection of humidity and temperature. The Fabry--Perot structure was fabricated through a modified version of the self-written waveguide technology, by employing a no--core fiber, while the PFBG was inscribed in a flat-sides microstructured polymer fiber (mPOF) using the phase mask technology through the 248 nm UV laser. The combination of these two polymer based technologies allow an easy fabrication and provide an efficient route for the simultaneous detection of humidity and temperature with high resolution.

OPTICS AND LASERS IN ENGINEERING 114, 37-43, 2019. DOI: 10.1016/j.optlaseng.2018.10.007

[P018-2019] "Structural and optical temperature-dependent properties of PbS thin films deposited by radio frequency sputtering"

da Silva, J. M. C.*; Marques, F. C.*

Lead sulfide (PbS) thin films deposited by radio frequency (RF) sputtering, in the 50-300 degrees C temperature range, were the subject of our investigation. We characterized the influence of deposition temperature on their structural, morphological, and optical properties by x-ray diffraction (XRD), atomic force microscopy (AFM), and UV-visible and Raman spectroscopy. XRD revealed that a transition from an amorphous to a crystalline structure occurs in the 200-250 degrees C temperature range. One was also able to observe an increase in grain size (determined by AFM), as the temperature increased. We also found that a broad range of band gaps (from 0.72 eV to 2.12 eV) might also be obtained by varying the deposition temperature.

MATERIALS SCIENCE IN SEMICONDUCTOR PROCESSING 91, 188-193, 2019. DOI: 10.1016/j.mssp.2018.11.029

[P019-2019] "Tm3+ doped Bi2O3-GeO2 glasses with silver nanoparticles for optical amplifiers in the short-wave-infrared-region"

Martins, M. M.; Kassab, L. R. P.; da Silva, D. M.; **de Araujo, C. B.***

We synthesized the Bi2O3-GeO2 (BGO) glass doped with thulium ions (Tm3+) and investigate the influence of embedded silver nanoparticles (Ag-NPs) on the samples photoluminescence (PL) and on the process of energy transfer (ET) among bismuth ions and Tm3+. The samples were prepared by the melt-quenching method with and without Tm2O3 and/or AgNO3. Under excitation at 808 nm the pure BGO glass presented PL from 1100 to 1500 nm, characteristic of the bismuth ions, Bi+, while the samples with Tm3+ exhibited a strong PL from 1300 to 1600 nm. The Bi+ emission was quenched due to ET from the bismuth centers to the Tm3+ and the emitted intensity at 1470 nm increased by more than 1000% due to the presence of Tm3+. Moreover, the samples with Tm3+ and Ag-NPs presented further PL enhancement of approximate to 56% at 1470 nm for the samples heat-treated during 2 h. Optical gain measurements using 2 mm thick samples were performed with a probe beam at 1470 nm and the pump beam at 808 nm. A 4.5 dB/cm gain in the presence of Ag-NPs was measured when the pump laser power was 6W. The Ag-NPs contributed to 500% of gain enhancement. The present results illustrate the appropriateness of the BGO glass with Tm3+ and Ag-NPs for obtaining intense PL and optical amplification in the near-infrared.

JOURNAL OF ALLOYS AND COMPOUNDS 772, 58-63, 2019. DOI: 10.1016/j.jallcom.2018.08.146

[P020-2019] "Topical essential fatty acid oil on wounds: Local and systemic effects"

Lania, B. G.; Morari, J.; de Almeida, A. R.; da Silva, M. N.; Vieira-Damiani, G.; Lins, K. A.; **Cesar, C. L.***; Velloso, L. A.; Maia, N. B.; Cintra, M. L.; Neves F. V. P. E.

Background: The use of medicinal plants and their derivatives is increasing, and approximately one-third of all traditional herbal medicines are intended for wound treatment. Natural products used in these treatments include vegetable oils, which are rich in essential fatty acids. Once in contact with an ulcerative surface, the oil reaches the blood and lymphatic vessels, thus eliciting systemic effects. Objective: This study evaluated the local and possible systemic effects of essential fatty acids (sunflower oil) applied topically to rat wounds. Methods: Cutaneous punch wounds (6 mm) were produced on the dorsa of 30 rats. Saline (SS), mineral oil (MO) or essential fatty acid (EFA) solutions were applied topically. Healing was evaluated after 2, 4 and 10 days (n = 5 per group) by visual and histological/morphometric examination, second harmonic generation (SHG) microscopy, and cytokine and growth factor quantification in the scar tissue (real-time PCR) and in serum (ELISA). Results: MO/EFA-treated animals had higher IGF-1, leptin, IL-6 and IFN-gamma mRNA expression and lower serum IL-6 levels than the control (SS/MO) animals. SHG analysis showed no difference in collagen density between the animals treated with MO and EFA. Conclusion: EFA treatment induces topical (observed by local IGF-1, leptin, IL-6 and IFN-gamma production) and systemic effects, lowering IL-6 levels in the serum. As the oil is widely used to shorten ulcer healing time, studies are needed to evaluate the treatment safety and possible undesired effects.

PLOS ONE 14[1], e0210059, 2019. DOI: 10.1371/journal.pone.0210059

[P021-2019] "Transverse momentum spectra and nuclear modification factors of charged particles in Xe-Xe collisions at root s(NN)=5.44 TeV"

Acharya, S.; Acosta, F. T.; **Albuquerque, D. S. D.*; Chinellato, D. D.*; De Souza, R. D.*; Takahashi, J.***; et. al.;
ALICE Collaboration

Transverse momentum (p(T)) spectra of charged particles at mid-pseudorapidity in Xe-Xe collisions at root s(NN) = 5.44 TeV measured with the ALICE apparatus at the Large Hadron Collider are reported. The kinematic range 0.15 < p(T) < 50 GeV/c and vertical bar eta vertical bar < 0.8 is covered. Results are presented in nine classes of collision centrality in the 0-80% range. For comparison, a pp reference at the collision energy of root s = 5.44 TeV is obtained by interpolating between existing pp measurements at root s= 5.02 and 7 TeV. The nuclear modification factors in central Xe-Xe collisions and Pb-Pb collisions at a similar center-of-mass energy of root s(NN) = 5.02 TeV, and in addition at 2.76 TeV, at analogous ranges of charged particle multiplicity density < dN(ch)/d eta > show a remarkable similarity at p T > 10 GeV/c. The centrality dependence of the ratio of the average transverse momentum < PT > in Xe-Xe collisions over Pb-Pb collision at root s= 5.02 TeV is compared to hydrodynamical model calculations.

PHYSICS LETTERS B 788, 166-179, 2019. DOI: 10.1016/j.physletb.2018.10.052

Artigos aceitos para publicação

[A001-2019] "High Performance of Carbon Nanotube Refrigerators"

Cantuario, T. E.; **Fonseca, A. F.***

Vapor-compression dominates the market for refrigeration devices due to low cost and relatively high efficiency. However, the most efficient vapor refrigerants are either ozone depleting or global warming substances. Solid-state cooling is a young field of research with promising results toward the development of new, efficient, and environment friendly technology for a new generation of refrigeration devices. One of these methods is based on the so-called elastocaloric effect (ECE), which consists of a temperature variation of a system in response to the application of adiabatic stresses. Although most of the literature describes the study of ECE solid-state cooling based on materials undergoing phase-transitions, a study recently predicted that carbon nanotubes (CNTs) present ECE as large as 30 K for 3% of strain.

This motivates research toward the development of nanorefrigerators. As nobody knows the efficiency of such an ECE-based CNT nanorefrigerator, here, significantly high coefficient of performance values of 4.1 and 6.5, and extracted heat per weight as large as 40 J g−1 are reported for a zigzag CNT nanorefrigerator operating in an Otto-like thermodynamic cycle. This efficiency is shown to overcome that of some other ECE materials.

Annalen der Physik, Article number 1800502, 2019. DOI: 10.1002/andp.201800502

***Autores da comunidade IFGW**
Fonte: Web of Science on-line (WOS)

Defesas de Dissertações do IFGW

[D001-2019] "Construção e Caracterização de um Sistema Óptico para Imageamento de Fluxo Sanguíneo"
Aluno: Leonardo Augusto Ulbrich Bueno
Orientador: Prof. Dr. Rickson Coelho Mesquita
Data: 20/02/2019

Fonte: Portal IFGW/Pós-graduação - Agenda de Colóquios, Defesas e Seminários.
Disponível em: http://portal.ifi.unicamp.br/pos-graduacao

***Nestes primeiros meses não há informações sobre Defesas de Teses do IFGW ou Defesas de Dissertações e Teses do PECIM.**

Fique por dentro!
Cadastre-se como leitor, e receba os avisos da publicação de novos números por e-mail.
<http://abstracta.ifi.unicamp.br>

Abstracta

Instituto de Física
Diretor: Prof. Dr. Pascoal José Giglio Pagliuso
Diretora Associada: Profa. Dra. Mônica Alonso Cotta
Universidade Estadual de Campinas - UNICAMP
Cidade Universitária Zeferino Vaz
13083-859 - Campinas - SP - Brasil
e-mail: secdir@ifi.unicamp.br
Fone: +55 19 3521-5300

Publicação

Biblioteca do Instituto de Física Gleb Wataghin
http://portal.ifi.unicamp.br/biblioteca

Diretora Técnica: Sandra Maria Carlos Cartaxo
Coordenadora da Comissão de Biblioteca: Profa. Dra. Arlene Cristina Aguilar

Elaboração:
Maria Graciele Trevisan (Bibliotecária)
Ayres Neri da Cunha Junior (Técnico Administrativo)
contato: infobif@ifi.unicamp.br